

Grain size variability on a rip-channelled beach

Edith L. Gallagher ^{a,*}, Jamie MacMahan ^b, A.J.H.M. Reniers ^c, Jenna Brown ^b, Edward B. Thornton ^b

^a Franklin and Marshall College, PO Box 3003, Lancaster, PA 17604, United States

^b Oceanography Dept., Naval Postgraduate School, 833 Dyer Rd, Monterey, CA 93943, United States

^c Rosenstiel School of Marine Science, University of Miami, 4600 Rickenbacker Causeway, Key Biscayne, FL 33149, United States

ARTICLE INFO

Article history:

Received 15 December 2010

Received in revised form 28 June 2011

Accepted 29 June 2011

Available online 21 July 2011

Communicated by J.T. Wells

Keywords:

grain size
beaches
digital imaging
nearshore

ABSTRACT

Grain size is an important variable when predicting beach morphodynamics. Beaches, to the eye, seem relatively uniform in grain size and morphodynamic modeling efforts usually assume a single mean grain size for an entire beach environment. Therefore, estimating grain size is traditionally done by collecting only a few samples and averaging to characterize the mean grain size of the whole beach. However, some studies have shown that even small variations in grain size can have a significant effect on model results when predicting beach morphology changes. Here, a mobile digital imaging system (DIS) has been developed for surveying spatial and temporal variation in grain size across a beach following the ideas of Rubin (2004). Using an off-the-shelf camera and underwater housing, macro photographs are taken of sand across a beach, which produce estimates of mean grain size that are highly correlated with estimates from sieves ($R^2 = 0.92$). High resolution maps of mean surface grain size are produced using the DIS (with ~1000 images over a 300×500 m area), which suggest that large variations in grain size exist (0.2–0.7 mm over tens of meters with accuracies of ± 0.03 mm) and that there is a correlation between spatial grain size variations and morphological variability.

© 2011 Elsevier B.V. All rights reserved.

1. Introduction

In the past, hydrodynamic and morphologic coastal modelers have assumed that the sand layer on the beach and shelf is thick, well sorted (uniform in grain size) and relatively smooth. Many field studies contradict this assumption. Gallagher et al. (1998) found that sediment grain size variation across the surf zone was an important factor in predicting profile evolution. MacMahan et al. (2005) found that surface sediment grain size varies depending on location in a rip current cell, potentially enhancing the morphodynamic feedback. McNinch (2004) found that the underlying geologic framework (eg, muds and gravels over areas of O[kms]) is exposed near hot spots (locations where the beach erodes dramatically, List et al., 2006) and hypothesized that different substrates cause anomalous nearshore processes such that wave attack is greater adjacent to the exposed substrate. Ardhuin et al. (2002) found that wave orbital ripple patchiness on the continental shelf is associated with grain size variations (with spatial scales <1 km). Trembanis et al. (2004) found that different ripple regimes, immediately adjacent to one another, were associated with different grain sizes. They also found that the wave friction factor (estimated from vertical velocity fluctuations) was significantly different for the two regimes and that it changed during storms. These patches of differing bed morphology have a significant effect on wave attenuation (Tolman, 1994; Ardhuin et al.,

2001). Large (O[100 m by kms]), regular, approximately shore-normal bedforms, known as rippled scour depressions, have been observed in 10–20 m water depth off many coasts (eg, South Carolina, Martha's Vineyard, west Florida, California: see Murray and Thielert, 2004 for a review) and are now thought to be sorted features, dependant on variable grain sizes and different bedform and roughness regimes. Grain size sorting is observed within beach cusps, exhibiting feedback between the flow and morphology (Komar, 1973; Antia, 1987). Within ripple and megaripple patterns, separation of grain sizes is also observed (Bagnold, 1941), with coarser grains found in troughs and finer sediments found on the crests. Rubin and Topping (2001) found that, in rivers, sediment transport can be more strongly regulated by changes in grain size than by changes in the flow.

These various studies suggest that sediment grain size in coastal (and other) environments is not homogeneous and that variations in sediment size and supply are important in sediment transport and morphodynamics from mm scales to km scales (hot spots, bars, rip channels, cusps, ripples, bedload transport). In addition, the feedback between the processes at small scales (eg, ripple formation, increased bed roughness and turbulence, winnowing of fine sediments) and the sedimentological framework reinforces the larger-scale morphological variability (eg, beach cusps, rip current cells, erosional hot spots or rippled scour depressions).

Unfortunately, measuring grain size is tedious and time consuming: in general, sediment samples need to be returned to the laboratory and measured. Traditionally, the measurement is done with sieves and involves drying, sieving (in this case we used quarter-

* Corresponding author. Tel.: +1 717 291 4055; fax: +1 717 358 4548.

E-mail address: edith.gallagher@fandm.edu (E.L. Gallagher).

phi interval sieves and samples were shaken for 10 min) and weighing. Some studies use fall velocity instruments or laser size analyzers rather than sieves. These also require sediment samples to be returned to the laboratory and prepared for analysis. Therefore, in spite of the evidence pointing to the importance of grain size in sand transport and morphodynamics on beaches, most of the studies mentioned earlier were based on relatively few field samples, painstakingly collected and subsequently analyzed in the laboratory. To capture detailed spatial and temporal variations in grain size using those techniques would be difficult and expensive. Here, a digital imaging system (DIS) is developed and tested to measure surface grain size in the nearshore. Following Rubin (2004), the 2D autocorrelation of digital, macro (very close-up) images of sediment is calculated and compared with calibration curves, to give an estimate of grain size. An examination of the measurement and image analysis techniques and associated uncertainties are presented here. With the DIS, many samples can be collected, more easily than with traditional techniques, allowing for high spatial and temporal resolution surveys. The DIS was used during field experiments in Truc Vert, France in May 2006 and March–April 2008, and in Monterey, CA in May 2007 and in April–May 2009. Maps of the spatial distribution of mean surface grain size before and after storms show that the DIS is capable of making detailed grain size measurements and that large variations in mean grain size are observed on natural beaches in both space and time.

2. The digital imaging system

2.1. Technique

The digital imaging system (DIS) used for this study consists of a Nikon D70 digital SLR camera with a 60 mm macro lens and three magnifying filters (+1, +2, and +4). This allows the camera to get within about 6 cm of the sand bed and capture images that are about 2.5×1.7 cm in size with a pixel resolution of $\sim 2000 \times 3000$. This camera is placed in an Ikelite underwater housing and, when taking pictures, the viewing port of the housing is placed directly on the sand bed. In doing this, the distance to the sand bed is fixed. Flexible LED

(light-emitting diode) strips, powered with three 9V batteries, are placed inside the housing to illuminate the sand bed immediately in front of the lens. This instrument is easy to handle in the field both while walking on the dry beach and while diving in deeper water.

Three example images of different sieved size fractions are shown in Fig. 1. Buscombe and Masselink (2008) examined a number of different numerical techniques for analyzing digital images of sediments. Here, we use the autocorrelation of the images following Rubin (2004). The lower panel in Fig. 1 illustrates how the autocorrelation curve, $r(l)$, depends on grain size. The correlation coefficient, r , resulting from horizontal offsets is given by

$$r(l) = \frac{\sum_{i,j} (x_{i,j} - \bar{x})(x_{i+l,j} - \bar{x})}{\sqrt{\sum_{i,j} (x_{i,j} - \bar{x})^2} \sqrt{\sum_{i,j} (x_{i+l,j} - \bar{x})^2}} \quad (1)$$

where x is the pixel intensity data from the image (which is converted to gray scale), i and j are the horizontal and vertical indices of the pixels (respectively), \bar{x} is the mean pixel intensity over the whole image, and l is the pixel offset (offsets from 0 to 100 pixels are shown in Fig. 1). Each image is divided into four sub-images (1150×500 pixels each) and, for each sub-image, both the horizontal autocorrelation (Eq. (1)) and the vertical autocorrelation are calculated. In this way, eight curves are calculated for each image and averaged. This technique improves statistical stability by increasing the number of independent estimates and by reducing the effects of anomalous grains while retaining a large number of grains in each sub-image.

For $l=0$, $r=1$, and, as l increases, r goes down. The resulting curve of $r(l)$ gives a statistical estimate of the coherent length scales in the image. For example, the correlation coefficient for the larger grains decreases slowly with increasing l , because the image remains correlated with itself for longer pixel offsets (Fig. 1, dotted curve). Conversely, r decreases quickly for smaller grains (Fig. 1, solid curve). The curves in Fig. 1 and others calculated from known size fractions are used to calibrate unknown autocorrelation curves derived from natural sediment samples. All of the calibration curves for two

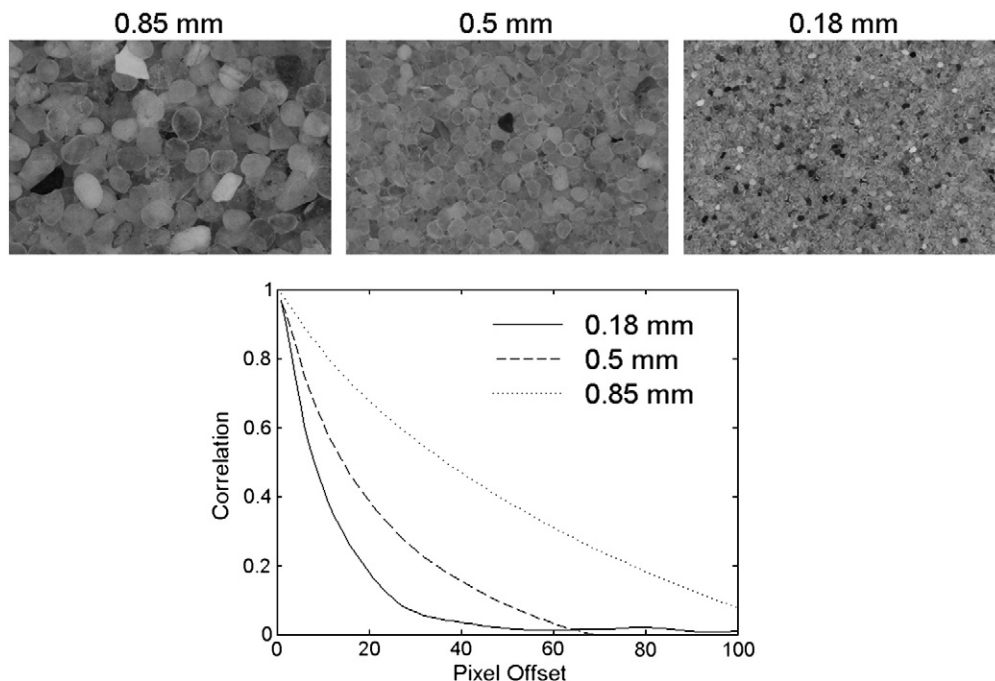


Fig. 1. A portion of each of three images of sieved sediment of three different sizes are shown in the top panels. The autocorrelation curves corresponding to the size classes in the images are shown in the lower panel.

different field experiments along with examples of natural images and their autocorrelation curves are shown in Fig. 2.

The calibration curves for each field site are developed by collecting one large sediment sample (~10 kg), drying and sieving that sample, and then using the DIS to photograph and generate autocorrelation curves for each of the known fractions. A large sample must be collected to produce enough sand to photograph at the extremes of the distribution (i.e., for the largest and smallest size fractions of which very little may be present on the study beach). The development of calibration curves for each study site captures the mineralogy, shape, color, and size distribution for a specific beach (Rubin, 2004). The variations between study sites are visible in the sample images and in their respective calibration curves, where curves representing the same size fraction look significantly different. Here, all calibration curves are averages of curves from at least 30 images taken in the laboratory with the sieved sands submerged in water. It has been found that many images of a single sample significantly improve the statistical stability (this is discussed in Section 2.2.1).

2.2. Analysis

2.2.1. Mean grain size

Mean grain size and the grain size distribution can be estimated quantitatively from the autocorrelation curves associated with natural, unsieved sands (which will be referred to as 'natural curves') and the calibration curves in different ways. The method used to calculate mean grain size for the field data presented later in this paper is to find the value of the natural curve at each pixel offset by linearly interpolating between the two nearest calibration curves (giving a size value for each asterisk in Fig. 2) and then averaging over all pixel offsets (Rubin, 2004). The number of pixel offsets over which to average can be varied. In these examples, the correlation curves run together for offsets larger than about 70, thus the important changes in the coherent length scales are represented best at lower pixel offsets. Maximum pixel offsets from 20 to 90 have been tested using images of natural samples that were

photographed in the field as well as being returned to the laboratory for testing. Four examples are shown in Fig. 3, with estimates of mean grain size using maximum pixel offsets from 30 to 60. These tests suggest that within a reasonable range of offsets, mean grain size is not sensitive to the maximum pixel offset used. For the data discussed later, a maximum pixel offset of 50 was used.

The interpolation technique for estimating mean grain size is robust, but the data can be noisy (Fig. 4). It has been found that multiple independent images of a given sample (or location) are necessary to produce a stable, dependable estimate of grain size. The minimum number of images necessary from a single sample for best results was found to be about 10. To determine number of images necessary, a single natural sediment sample (~200 g) was photographed in the laboratory 100 times. Using these 100 images, mean grain size was calculated from a random selection of 1–30 images repeatedly. The results of this analysis suggest that variations in estimates of mean grain size were large for fewer than about 10 images (Fig. 5). The 90% confidence interval in the estimate of mean grain size is calculated as $ci = 1.65 \times std / \sqrt{N}$ where N is the number of independent mean grain size estimates and std is the standard deviation (Fig. 5b). Note that each image is broken into 4 sub-images, as in Fig. 2, and both horizontal and vertical autocorrelations are performed, so $N = 8 \times$ number of photographs taken. This calculation of confidence interval is used as a measure of grain size uncertainty for the field data presented in Section 3. The percent error of the mean is calculated as

$$percenterror = \frac{1}{N} \sum_{i=1}^M \frac{\sqrt{(x_i - \bar{x})^2}}{\bar{x}} \quad (2)$$

where x_i are estimates of mean grain size from individual photos, the overbar denotes the mean of all x_i and N is the number of photos. Percent error is shown in Fig. 5c and similarly suggests that for more than about 10 images the uncertainties converge to something between 10% and 15% of the mean.

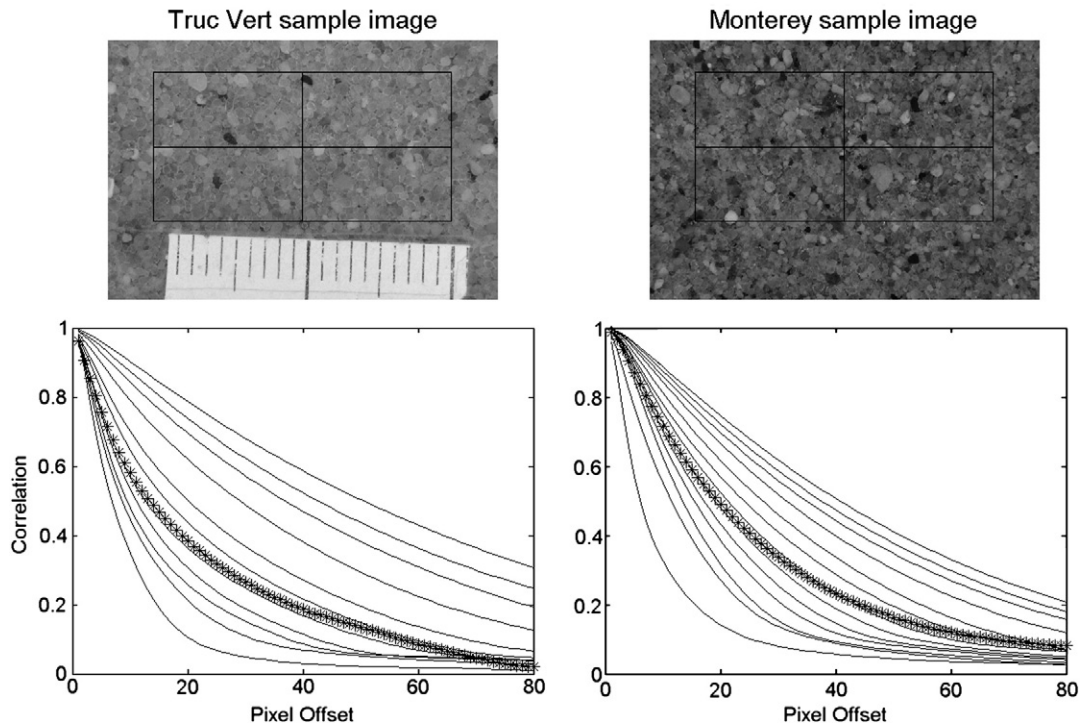


Fig. 2. Images of natural sand and their corresponding autocorrelation curves (asterisks) from Truc Vert (left panels) and Monterey (right panels). The solid lines are the calibration curves, calculated from images of sieved sand (eg. Fig. 1), which is taken from each field site, sieved and photographed. Moving from top to bottom, the calibration curves correspond to sand sizes (left panel, Truc Vert) 1.18, 1.0, 0.85, 0.71, 0.6, 0.5, 0.425, 0.355, 0.3, 0.2, 0.125 mm and (right panel, Monterey) 1.4, 1.18, 1.0, 0.85, 0.71, 0.6, 0.5, 0.425, 0.355, 0.3, 0.25, 0.18, 0.15 mm.

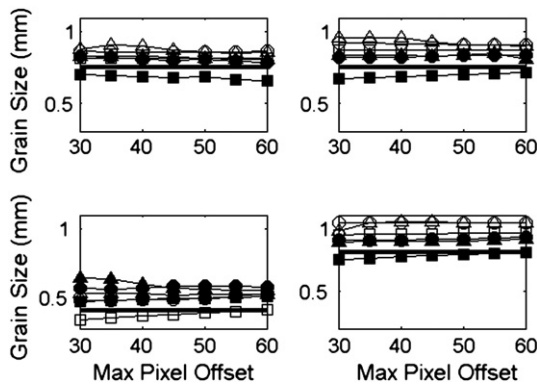


Fig. 3. Mean grain size plotted as a function of maximum pixel offset used. The thick solid black line represents mean grain size estimated from the sieved distributions and is considered the true mean grain size. Squares represent estimates of mean grain size using the interpolation technique of Rubin (2004). Estimates of mean grain size using Eq. (3) and the distributions calculated with the MEM method are shown as triangles and calculated with the LSQ method are shown as circles. Filled symbols represent estimates from photographs taken in the field when the samples were collected. Open symbols represent estimates from photographs taken in the laboratory with the sample submerged in water.

The percent error as calculated earlier represents uncertainties associated with estimates of grain size from both natural variability in the sample of sand and from errors in the technique. Barnard et al. (2007) did a similar analysis by taking many images of a single location ($\sim 1 \text{ m}^2$) on a beach and they also found that multiple images were needed to given a stable estimate of mean grain size. They found that with greater than about 20 images, the percent error of the mean was reduced to less than 5% (their Fig. 9). The minimum values for percent error here are a bit higher, with 10%–15% uncertainty for the natural sand samples (unsieved). It is possible that the natural variability of their surface sample location was lower than that of the samples tested here. Rubin et al. (2007) showed that sediments just below the sand surface on bars along the Colorado River in the Grand Canyon were significantly different than sands on the surface. The sediment sample discussed here was scraped from the top $\sim 5 \text{ cm}$ of beach sand. To test these ideas about horizontal or vertical spatial variability, a similar analysis was done with sand that had been sieved for calibration, thus removing natural variability. A sample of sand from the $710 \mu\text{m}$ sieve (ie, sand sizes between 710 and $850 \mu\text{m}$) was photographed 100 times and percent error was found to be 6% (9% for $850 \mu\text{m}$ sand and 11% for the $1000 \mu\text{m}$ sand. Note that the range of

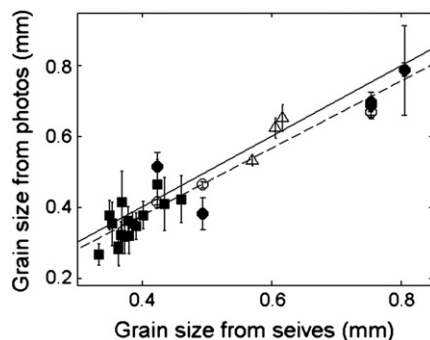


Fig. 4. Mean grain size estimated with the DIS (using Rubin's (2004) interpolation method) plotted versus mean grain size calculated from the sieved distribution using Eq. (3). Circles are from Monterey, triangles are from an early experiment in Sennen, England in 2005 and squares are from an early experiment in Truc Vert France in 2006. Open symbols are samples that were photographed in the laboratory (and are generally from many photographs), filled symbols are samples that were photographed in the field (and generally are from only a few photographs). The solid line shows the one-to-one relationship and the dashed line shows the best fit line with the correlation coefficient of $R^2 = 0.92$. Bars represent 90% confidence interval as calculated for Fig. 5.

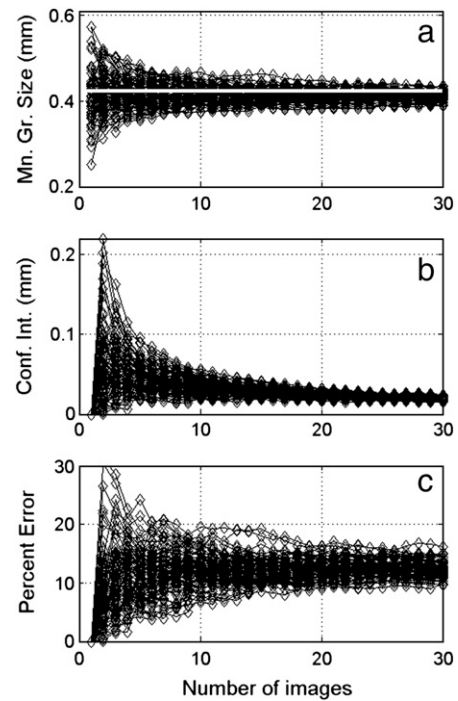


Fig. 5. a) Mean grain size, b) 90% confidence interval and c) percent error plotted versus the number of images used in calculating mean grain size. The horizontal white line in panel a) represents the mean grain size for this sample calculated from the sieves.

sizes in each sieve is increasing). So, using the present system with narrowly distributed sand still results in percent errors larger than those of Barnard et al. (2007).

Although the system used in the present study, seems to have slightly higher systematic errors than those used by Barnard et al. (2007), Rubin et al. (2007) and colleagues, it is clear that within a reasonable range of uncertainties, these digital imaging systems can estimate grain size well and extremely efficiently. Mean grain size estimates (Fig. 5, Barnard et al., 2007 Fig. 9) begin to converge when 10–15 photographs are taken, which is suggested here as the minimum number of images for obtaining a statistically stable mean grain size. In addition, taking more images only adds seconds to the processing time (Barnard et al., 2007). For the field data analysis presented in Section 3, confidence interval is included with the spatially averaged result to elucidate the total uncertainties (natural variability and technique error) in those measurements.

2.2.2. Grain size distribution

The distribution of grain sizes in a single sample has been calculated by two techniques. A non-negative, least-squares regression (LSQ) of the natural autocorrelation curve with the calibration curves following Rubin (2004) finds the fraction of each of the calibration curves that is represented in the natural curve, giving a distribution (or percentage) of each grain size contained in the natural sample (Fig. 6a and b). A maximum entropy method (MEM, see Appendix A or Lygre and Krogstad, 1986) has also been tested as a technique for fitting the natural curve to the calibration set (Fig. 6c and d). As with the mean grain size estimate, only the portion of the autocorrelation curves between 0 and 50 pixel offsets is used to calculated distribution for this study.

The results of estimating grain size distribution are also noisy. Grain size distributions estimated from single images can produce widely varying results. These individual and often anomalous distribution estimates are shown as thin dotted lines in Fig. 6. The thin solid lines in Fig. 6 are the individual distribution estimates from the images in Fig. 2 and are good examples of how the individual distribution estimates sometimes do not correspond to the true distribution (from sieves, thick dashed line with circles). As with the estimates of mean grain size, the

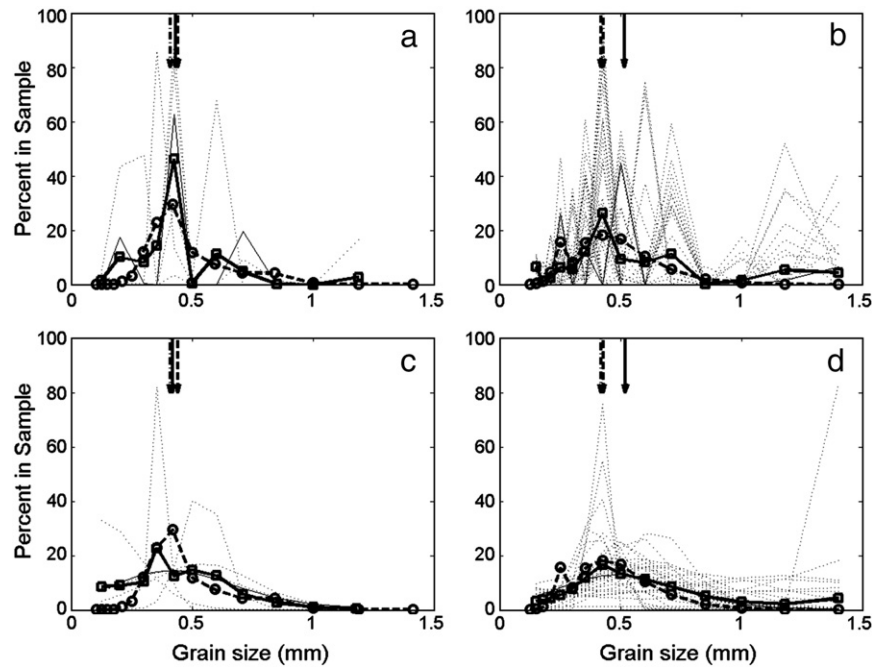


Fig. 6. Examples of grain size distributions estimated with the DIS a) and c) from Truc Vert, France (2006) and b) and d) from Monterey, CA. In a) and b) grain size distribution is calculated using the LSQ fitting routine and in c) and d) distribution is calculated using the MEM fitting routine. The thin dotted lines are distributions estimated from individual photographs. The thick solid line with squares is the average of all the thin lines in each plot and represents the mean distribution estimated by the DIS. The thick dashed line with circles is the distribution measured with sieves. The arrows are mean grain size values estimated 1) by linear interpolation of the autocorrelation curve with the calibration curves following Rubin (2004) (dash-dot), 2) from the camera-estimated distributions following Eq. (3) (solid), and 3) from the sieved distribution (dashed). The photos and resulting thin dotted curves in the Truc Vert examples (a and c) were from an early field experiment and only a few good photos were collected at each location (here there are 6). In the Monterey examples (b and d), the sand sample was returned to the laboratory for analysis, so many photos were taken (about 30 are shown). The thin solid lines are the distributions that correspond to the individual photos in Fig. 2.

average of many distribution estimates from many images of a single sample or location can often generate a realistic estimate of distribution (thick solid lines with squares in Fig. 6). In Fig. 6a and b, the distributions are calculated from the LSQ method. The LSQ method often produces individual distributions (thin dotted lines) that include peaky bimodality or large or small fractions which do not exist in the sample at all. In Fig. 6c and d, distributions of the same two samples are calculated from

the MEM method. The MEM method was employed to try to obtain smoother, more realistic estimates of distribution. The individual estimates (thin lines) are indeed smoother, but the final distribution estimates are not more accurate than those obtained with the LSQ method.

Unfortunately, even after averaging, sometimes the distribution estimates can be different from known grain size distributions. In

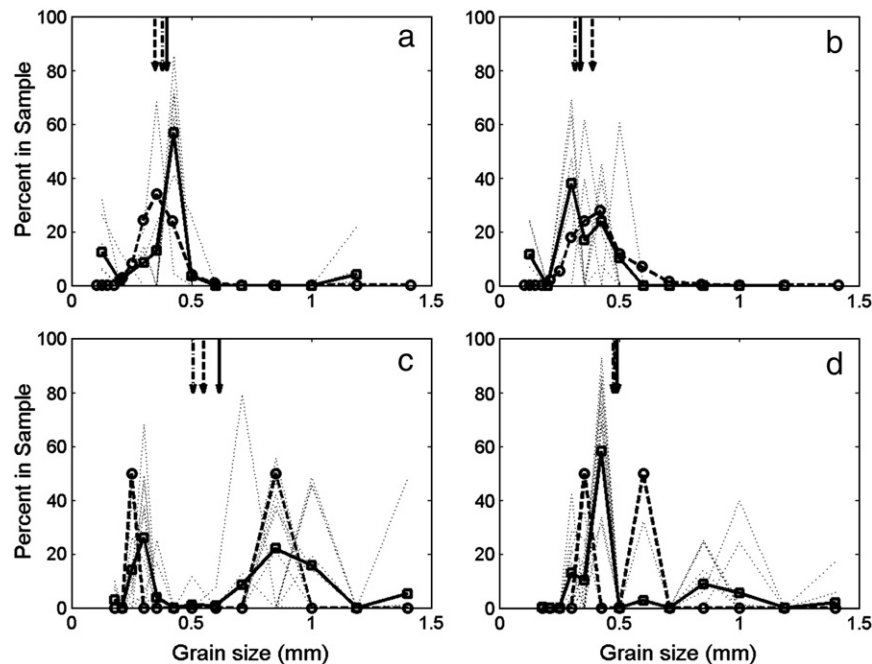


Fig. 7. Examples of poorly estimated distributions. a) and b) are samples from Truc Vert, France (2006) and c) and d) are bimodal distributions created in the lab from sieved sands. In all panels the DIS distribution was calculated using the LSQ fitting method. Symbols and lines are the same as in Fig. 6.

Fig. 7, more examples of distributions are shown. These were chosen to illustrate problems that are often encountered with distribution estimates. A common problem is that the magnitude of the peak in the estimated distribution is too large or does not correspond to the peak in the true distribution (Fig. 7a). An inaccurately peaky or bimodal distribution estimate, when the true distribution is smooth and regular, is also common (Fig. 7b). In both Fig. 7a and b there is also an anomalous peak at 0.125 mm that is not in the sample at over 10%. Peaks at the smallest and largest fractions are a common anomaly of the LSQ technique. The distributions in Fig. 7a and b are field samples from Truc Vert, France and the DIS estimated distributions do not represent well the true distribution. As with Fig. 6a, these were photographed in the field and the samples were returned to the laboratory for sieving.

Because the natural samples earlier were basically unimodal, known sieved sands were combined to create bimodal distributions and their distributions were estimated with the DIS (Fig. 7c and d). In general, this test produced good results for distributions where the two modes were similar (like the natural samples discussed earlier). However, when very large and very small grains were combined to give strong bimodality, the DIS gave mixed results. In Fig. 7c, the sense of the bimodality is reproduced, but the amplitudes of the two peaks are not accurate. In addition, the peak at 1.4 mm represents a fraction that did not exist in the man-made sample. In Fig. 7d, the DIS estimate does not reflect the bimodality at all. A general sense of the range of grain sizes and approximate mean can usually be obtained from the distributions estimated from the photographs. However, they are not accurate enough for obtaining subtle details about the grain size distribution.

Buscombe (2008) used a kernel density filtering technique to improve (LSQ) estimates of grain size distribution. Working with images of sediments from gravel beaches, he found that distribution estimates could be smoothed and improved. From these distribution estimates, he obtained more accurate higher-order grain size statistics (kurtosis and skewness), but that even with the new technique, the shape of the distribution was “not always mimicked exactly”.

As discussed earlier, mean grain size was calculated directly from the autocorrelation curve by interpolation with nearest calibration curves and averaging. Mean grain size also can be calculated from the

DIS estimated grain size distributions. The value of mean grain size (\bar{D}) is calculated from a distribution using

$$\bar{D} = \frac{1}{100} \sum_{i=1}^M (sc_i \times p_i) \quad (3)$$

where M is the number of size classes used, sc is the value of each size class (in mm) and p is the percentage of the total distribution contained in that size class. Eq. (3) is used to calculate mean grain size for the sieved samples in this study and mean grain size can be calculated in this way from the distributions estimated from images (using either LSQ or MEM methods). The values of mean grain size calculated from the DIS distributions can vary widely, likely owing to the inaccuracies of those grain size distributions (compare arrows in Figs. 6 and 7). For example, in Fig. 6b and d, both the LSQ and the MEM distributions have anomalous fractions above 1 mm, which contribute to an anomalously high estimate of mean grain size (solid arrows). For the remainder of this paper we will use the estimate of mean grain size from the interpolation routine, following Rubin (2004). Although this value for mean grain size can also vary from the true value, it tends to be closest to the true value ($R^2 = 0.92$, Fig. 4).

2.3. Field considerations

The primary source of error in estimating grain size is poor focus of the digital images. The camera was focused manually in the present study, because the auto-focus function on the camera did not produce consistent results. Thus, there are two causes of poor focus: 1) motion and 2) a slight change in actual distance of the camera from the sand resulting from the focus being set slightly differently from one batch of images to another. Working in a dynamic environment means sometimes the camera, the diver, or the sand will be in motion, resulting in poor focus. Fig. 8 shows an example of the effect of motion on the focus and the resulting estimate of grain size. These images were taken in the laboratory with the camera held against the sand in a bowl and then the bowl was rotated slowly or quickly. The center of rotation can be seen as the small patch that remains in focus. Although the rate of rotation was not quantified, an intuitive sense of the strong dependency on proper focus can be gained from this example. A change in focus

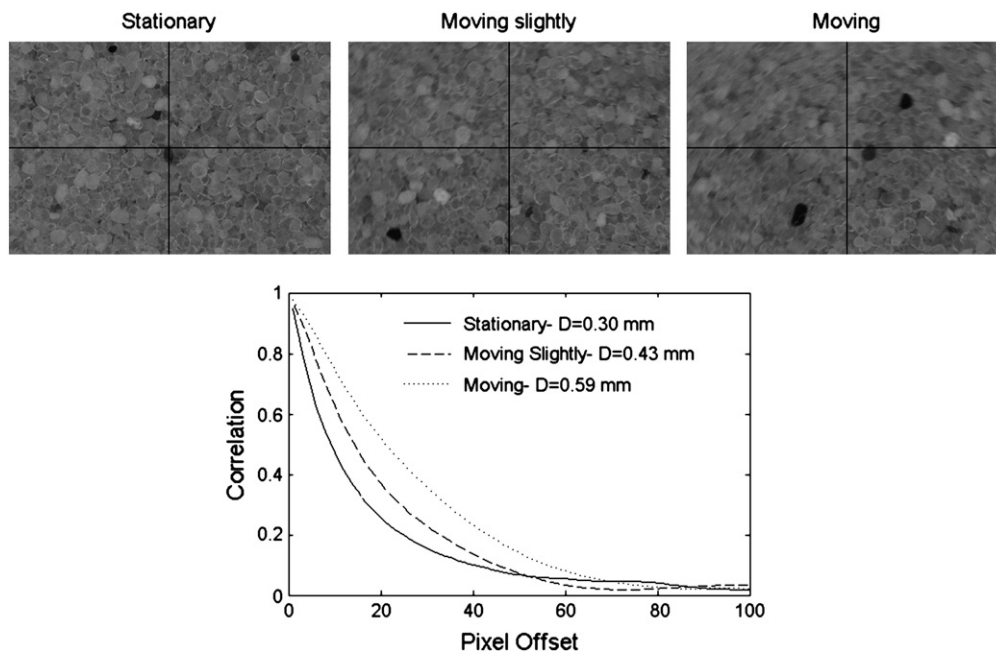


Fig. 8. Focus test. Top panels show images of a single sand sample stationary and in focus, moving slowly and slightly out of focus, and moving quickly and very out of focus. In the bottom panel, the autocorrelation curves for those images are shown to illustrate how focus affects mean grain size estimates (\bar{D}).

owing to motion can produce errors of 25% or more. Caution while sampling in the field and careful quality control to eliminate bad images are used to eliminate errors owing to motion while sampling.

Poor focus owing to slight changes in distance to the bed is a more insidious problem. The accuracy of the technique depends on the camera being a fixed distance from the bed for both the calibration and the natural images. Because, with the prototype instrument, the focus was set manually, the focus could be slightly different before and after camera maintenance (battery or memory card changes). Similarly, if the focus knob is bumped during a survey, small systematic changes will occur in the results. A slight focus change like this resulted in an offset in grain size of 0.1 mm before and after camera maintenance at an early experiment at Truc Vert, France in May, 2006. During subsequent experiments the camera was always focused using images of measuring tapes. For some experiments small pieces of measuring tape were actually attached to the housing lens so that the tape is in every image (Fig. 2 top left). This ensures focus and eases quality control. This temporary fix often came off during surveys (eg. Fig. 2 top right) and was replaced by images of a loose measuring tape at the beginning and the end of a survey to ensure consistent focus. In later DIS generations, a permanent scale, visible in every image, will be designed into the housing.

Because the autocorrelation technique involves de-meaning the images, light levels do not change grain size estimates and light levels do vary over the course of a survey. For example, fresh batteries provide strong lights that gradually become dimmer over the course of a survey as battery power wanes. Similarly, dry sand on a sunny day can be lighter than submerged sand which is darker and receives almost no ambient light. (Not much light enters the housing from outside, when the lens is pressed against the sand, but there is some.) Camera settings, like aperture and shutter speed, can be changed to optimize light levels; these settings do not affect the autocorrelation or results. However, slow shutter speeds can result in image focus problems owing to motion, and a low f-stop value (a measure of aperture), while increasing light, decreases the depth of field or the depth over which the image is in focus. Because focus does affect the estimate of grain size, higher f-stop values are desirable. It is recommended that anyone wishing to use this technique should become familiar with basic photographic techniques and constraints.

Unfortunately, sand that is slightly damp causes a visual clumping of grains and sometimes liquid puddles (in partially dry/partially wet sand) can obscure the image. The region at the top of the swash on a beach that is periodically wet then dry was avoided (by working with the rising or falling tide) owing to this image deteriorating effect.

3. Field results and discussion

The DIS has been used in a number of field experiments. Here, results from a multi-institutional experiment at Truc Vert, France in March and April 2008 will be shown. Truc Vert beach is macro-tidal with an annual mean spring tide range of 3.70 m. The wave climate is moderate with an annual mean significant wave height of 1.36 m and mean period around 6.5 s, but there is a strong seasonal dependence. During the 2008 experiment under storm conditions, offshore significant wave heights reached 8 m (measured in 20 m depth). The morphology of the beach is complex, three-dimensional and highly dynamic. The inner, intertidal bar has a transverse bar/rip morphology (Senechal et al., 2009), shown in Fig. 9 and during this study, this morphology was observed to migrate from north to south owing to large waves from the northwest. The outer, subtidal bar is persistently crescentic with an average wavelength of about ~715 m (Castelle et al., 2007).

During this experiment, the DIS was used to make large (300×500 m) spatial surveys of surface grain size over the inner, intertidal bar region at low tide. Positions of the photographs were determined by time-syncing the camera images with a small GPS that was worn by the surveyor. The GPS was post-processed to give horizontal accuracy of about 10 cm (MacMahan et al., 2009). The vertical accuracy of

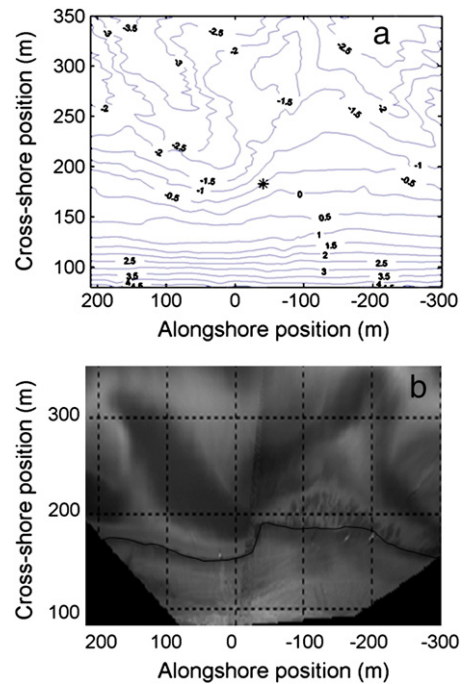


Fig. 9. a) Bathymetry measured on March 19, 2008 using a survey-grade GPS system mounted 1) on a jet-ski with a depth finder for subaqueous sampling, 2) on a person walking for shallow water measurements and 3) on an ATV for dry beach measurements. See MacMahan (2001) for more details on bathymetric surveying. Asterisk shows location of fixed instrument frame where measurements in Fig. 15 were made. b) Time lapse video image of the intertidal region (approximately the same region covered in panel a) at Truc Vert on March 19. The black line indicates the water line, offshore of which shallower areas are lighter owing to wave breaking, and deeper areas are dark with no breaking. In this image there are distinct deep areas corresponding to the transverse rip feeder channels. North is to the right and offshore is up in the image.

the GPS used with the camera was not sufficient for measuring bed elevation. Separate high-resolution surveys of the morphology were completed with a kinematic, DGPS system (MacMahan, 2001; Senechal et al., 2009). During the 3 week experiment, five surveys of grain size and two bathymetric surveys were completed (Fig. 10). Despite the

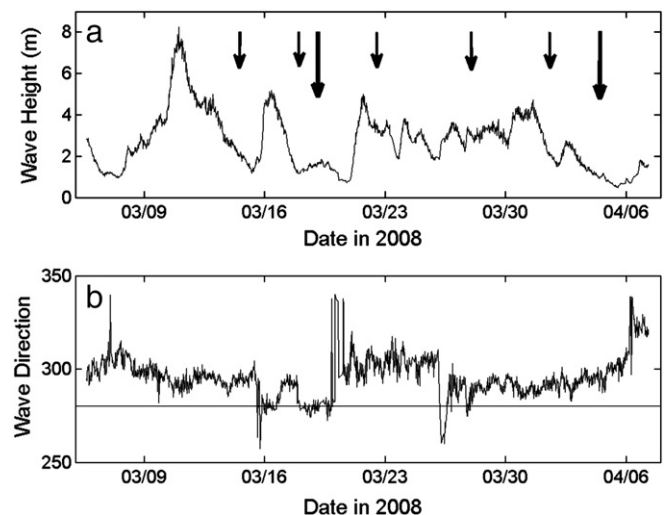


Fig. 10. a) Significant wave height measured in 20 m water depth offshore of the Truc Vert field site. Shorter arrows indicate times of DIS surveys, larger arrows indicate times of bathymetric surveys. b) Wave direction in degrees measured in 20 m water depth. The horizontal line at 280° represents the shore normal wave approach and angles greater than 280° represent wave approach from the north.

convenience of the DIS, working around large waves and rising tides, and covering a large intertidal area was still found to be time consuming, thus some of the surveys took multiple days to complete (by a single person surveying). For example, the intertidal shoals were only available at the lowest spring tides and then only for ~2 h surrounding the low tide. On dry ground a location could be sampled about once every 2 min (including taking 10–15 photos and moving from one point to the next), in the water, this process is slower. The results of the first survey, conducted on March 14 and 15, are shown in Fig. 11. On March 14 about 1100 images were collected (taking about 4 h to complete) and on March 15 more than 600 images were collected (taking about 2 h to complete). Once examined for acceptable focus (which takes about 1 hr for 1000 images) there were 1058 images available to estimate grain size. In Fig. 11a, the estimates of mean grain size from all 1058 photos are represented by the color of the symbols. For Fig. 11b, all those estimates

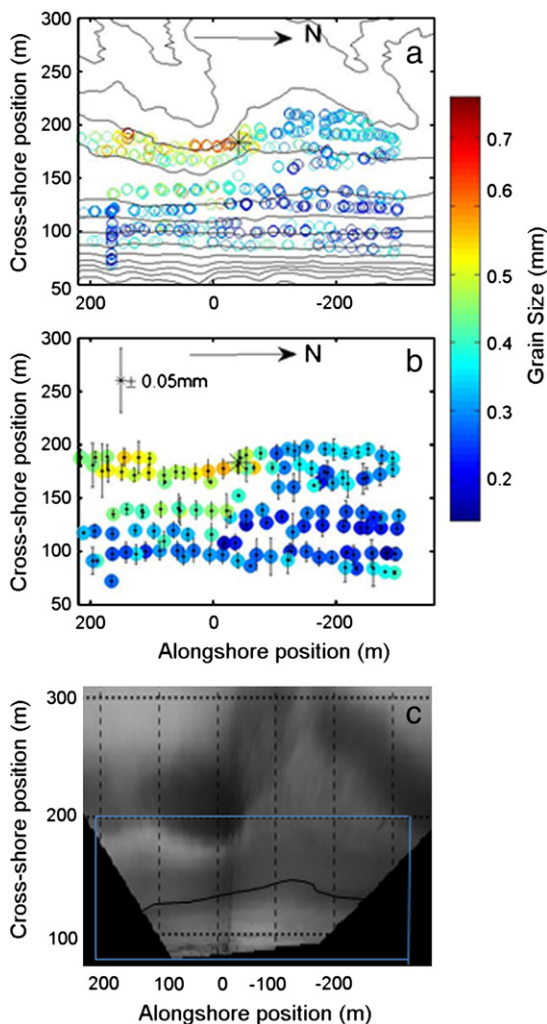


Fig. 11. a) Circles give the position of individual photographs (there are 1058) taken during the March 14/15 DIS survey at Truc Vert, France and contours represent bathymetry measured on March 19 (same as in Fig. 9a). The color of the circles indicates the mean grain size. b) The data in a) were grouped into 20×20 m bins and averaged (color of large dots indicates grain size). The bars represent the 90% confidence interval for the grain size estimate at each 20 m^2 bin where photos were taken. (Confidence interval calculated as in Fig. 5.) Asterisk shows location of fixed instrument frame where measurements in Fig. 15 were made. c) Time lapse video image of the intertidal region (approximately the same region covered in the top panels) at Truc Vert on March 14. The thin white lines outline the region that was surveyed with the DIS. The black line indicates the water line, offshore of which shallower areas are lighter owing to wave breaking, and deeper areas are dark with no breaking. North is to the right and offshore is up in the image.

from individual photos are averaged in 20 m^2 bins and the bars represent the 90% confidence interval. This map of confidence is typical of all the surveys collected, where most estimates of mean grain size on the 20 m^2 grid are good to less than $\pm 0.02 \text{ mm}$, but a few have bars as large as $\pm 0.05 \text{ mm}$. Recall that these uncertainties are owing to both natural variability in the region being sampled and small technique errors.

In Fig. 11a, the bathymetry from March 19 is also plotted as black contours. The coarse region near $x = 0 \text{ m}$ and $y = 200 \text{ m}$ corresponds to the head of a rip channel, while the mean grain size on the shoal between the two rip channels is finer. The higher and drier part of the beach, which is often subjected to aeolian transport, tends to be finer than either the rip or the shoal. This pattern was regularly observed on this beach and has been observed on other beaches as well (MacMahan et al., 2005). Thus, the grain size variations across the study region are observed to vary with the local morphology. In Fig. 11c, a time lapse video image of the intertidal region from March 14 is shown. These images provide a general view of the subaqueous morphology when bathymetric surveys are not available (Lippmann and Homan, 1989), because waves breaking in shallow water appear lighter in color, whereas deeper areas are darker without breaking waves. In Fig. 11c, the deep rip channel, where the coarse sediments are observed, in the southern half of the study region, is clearly visible.

Although the March 14/15 DIS survey and the March 19 bathymetric survey were separated by a large wave event (Fig. 10, March 16–17), those waves were approximately shore-normal, so the alongshore position of the southerly rip channel did not change significantly. This was verified by examining time lapse video images. However, the coarse sediments associated with the head of the rip channel migrated shoreward (compare Figs. 11b and 12a), suggesting that the steep edge of the channel also moved onshore (Fig. 13a). Small changes in bathymetric patterns like this (depth changes or small onshore-offshore motion) are difficult to assess from the video images, because the images are based on wave breaking patterns, which change with the tides and wave height.

The morphology of the more northerly rip channel was changed significantly during this storm (compare Figs. 11c and 13a). Casual observations from the beach, as well as a coarsening of mean grain size across the shoal and along the edge of the northern rip channel (Fig. 12a) suggest that the northern channel moved closer to shore. (This is accurate for the portion of the channel closest to the beach. Further offshore some very interesting and unusual changes occurred in the northern rip channel, but unfortunately these are not covered by the present data set). Note that the DIS survey in Fig. 12a was collected over the course of four days (March 17–20) and although the waves were less than 2 m, the dynamic beach continued to change. This may explain some contradictory data points.

Mean grain size was surveyed again on March 22–23 during the next large wave event. At this time the wave approach was strongly from the north (Fig. 10) and the more northern rip channel and next shoal to the north were observed in the field to be actively migrating, with a slip face along the northern edge of the rip channel (as if the northern shoal was a large bedform migrating into the channel), and large megaripples (60–80 cm in amplitude) were migrating within the rip channel. During this survey the tide was low enough (despite the large waves) to make measurements in the northern rip channel itself. Interestingly, the 20 m^2 bin-averaged grain size in the rip channel was only slightly coarser than on the adjacent shoals (Fig. 12b). Zooming in on the rip channel region from that survey, the data from the individual photographs are shown in Fig. 14a and they suggest that there are extremely large variations in grain size with large sediments ($\sim 0.6 \text{ mm}$) as well as much finer sediments ($\sim 0.3 \text{ mm}$). When this combination of coarse and fine sediments in the region are averaged in 20 m^2 bins they give a misleadingly smooth grain size map, but if averaged over smaller 5 m^2 bins, the high spatial variability in grain size over small distances is striking (Fig. 14b), albeit with fewer images and a larger confidence interval. Although a pattern is not resolved with these measurements, it

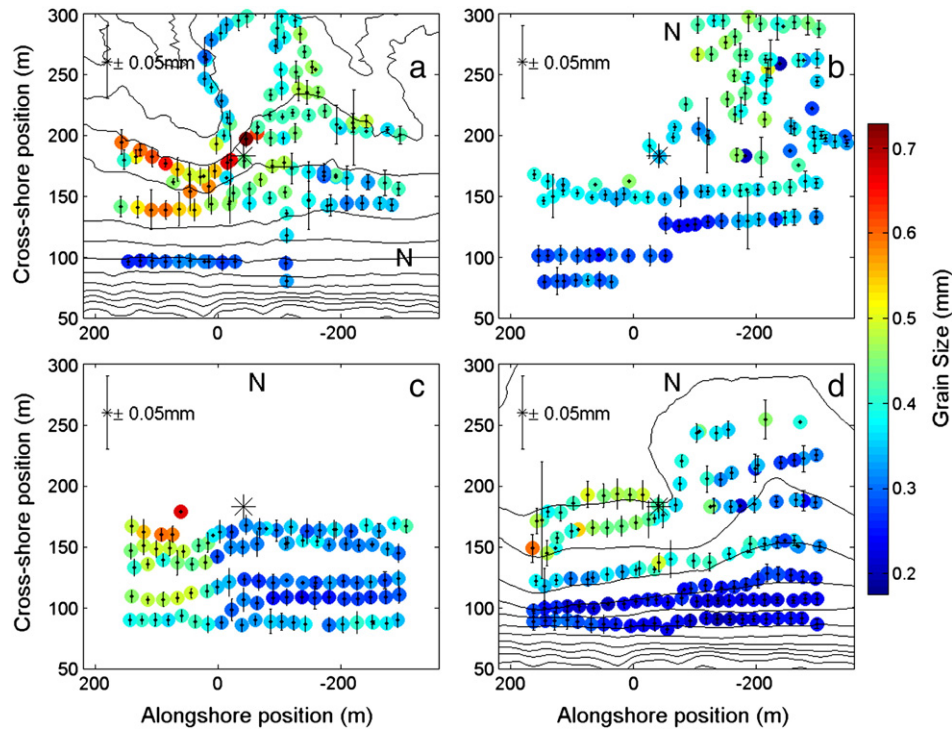


Fig. 12. Maps of mean grain size at Truc Vert beach averaged in 20×20 m bins from a) March 17–20, b) March 22–23, c) March 28 and d) April 1–2. Contours in a) and d) represent bathymetry measured on March 19 and April 4, respectively. Bars represent 90% confidence interval. The asterisk in each panel shows the location of the fixed instrument frame where measurements in Fig. 15 were made.

is likely that the large megaripples were finer sediments from the shoal migrating across the coarse floor of the rip channel, which was still visible (and measureable) underneath.

Large waves made it impossible to sample in the deeper southerly rip channel during the March 22–23 survey and, although the time lapse images suggest that it is still in approximately the same position, the

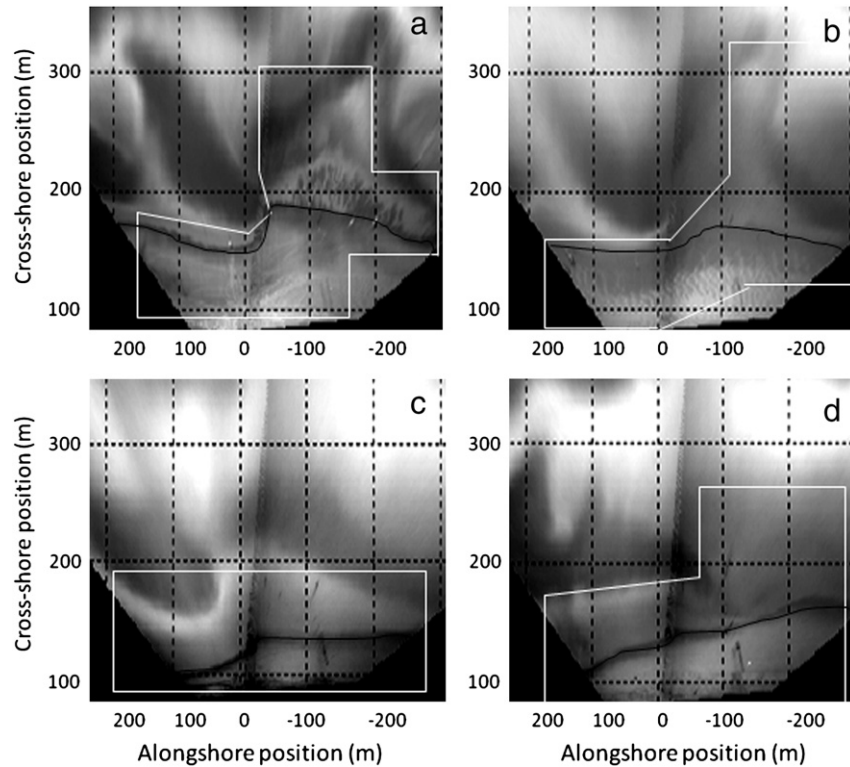


Fig. 13. Time lapse video images of the intertidal region at Truc Vert during each of the four DIS surveys (Fig. 13) a) March 17–20, b) March 22–23, c) March 28 and d) April 1–2. The thin white lines outline the regions that were covered by the DIS on each day. The black line indicates the water line, offshore of which shallower areas are lighter owing to wave breaking, and deeper areas are dark with no breaking. North is to the right and offshore is up in the image.

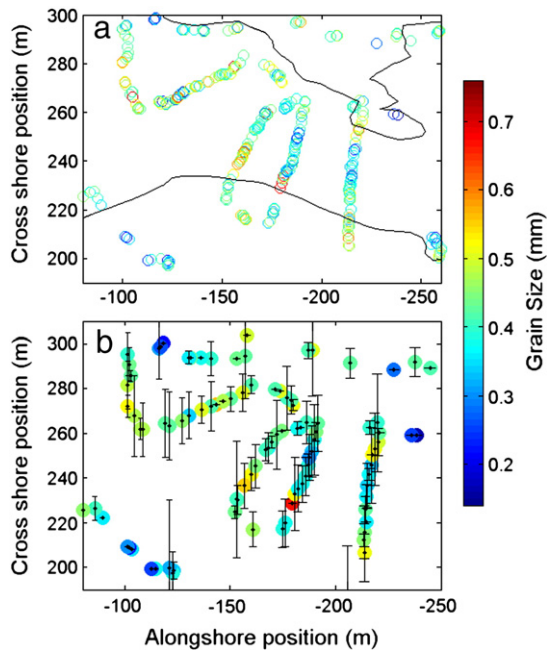


Fig. 14. Close up of the northern rip channel from the March 22–23 survey. a) Circles give the position of individual photographs, with color representing the grain size. Contours show northern rip channel bathymetry from March 19, note that on March 22–23 the channel has migrated to the south (left) and the back-and-forth photo survey lines cross the center of rip channel. b) Grain size from individual photos was averaged in 5 m² bins and the bars represent the 90% confidence interval for the grain size estimate at each 5 m² bin where photos were taken. Large gradients in grain size are now visible with the smaller averaging area.

grain size data are finer near its edge than in the previous survey, suggesting that the channel may have moved offshore slightly.

The next survey was conducted on March 28, after a few days of large ~3 m waves that were predominantly from the northwest (Fig. 10). The time lapse image suggests that the northern rip channel continued to move toward the shore and to the south (Fig. 13c). The deep coarse southerly rip channel also moved to the south as indicated by both the time lapse images (Fig. 13c) and the mean grain size patterns (Fig. 12c). This DIS survey is less extensive because it was during the neap tide and the shoals were not accessible.

The final DIS survey was conducted on April 1 and 2. The waves had finally begun to settle after being ~3 m high for approximately 10 days (Fig. 10). The time lapse images suggest that the northern rip channel continued to migrate to the south and joined the more southerly rip channel, giving one large shoal and one large, broad rip channel in the study region (Fig. 13d). This is reflected in both the bathymetry (measured on April 4) and in the mean grain size pattern where coarse sediments are associated with the channel to the south and finer sediments are observed on the shoal to the north (Fig. 12d).

The large-scale spatial surveys are time-intensive and dependant on conditions, so to support those data, images were taken every day at a fixed location to better capture temporal variations in grain size. The location of those daily samples is marked in the images in Figs. 9, 11 and 12 with a black asterisk (at $x = -40$ m and $y = 190$ m) and is near a fixed instrument frame. The time series of daily mean surface grain size at that location is shown in Fig. 15. This instrument frame was deployed on March 15 just northward of the southerly rip channel head and at that time the mean grain size was relatively coarse at more than 0.5 mm. During the course of the experiment the fine sediments of the shoal to the north of the instrument frame migrated to the south and almost completely buried the sensors on that frame. At that time the mean grain size was less than 0.3 mm. As the morphological system continued to change with the northern rip moving in and welding to the southern rip channel, the fine sediments of the shoal moved out from beneath the

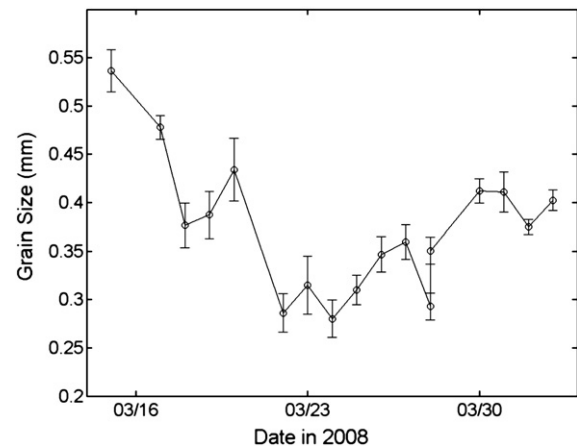


Fig. 15. Mean surface grain size measured daily at a fixed instrument frame during the Truc Vert 2008 field campaign plotted versus time.

frame and the coarser sediments of the northern rip channel came into the region with a mean grain size of ~0.4 mm.

4. Conclusions

Sediment transport is a function of fluid strength and grain size, therefore the ability to predict morphodynamic processes at any scale depends on a complete picture of spatial grain size variability. To this end, a mobile hand held digital imaging system (DIS) has been developed (following Rubin, 2004) to facilitate the collection of both high spatial and high temporal resolution surface grain size information in the nearshore. The imaging system has been tested carefully and shown to be useful for measuring mean surface grain size. However, estimates of grain size distribution tend to be inaccurate using both Rubin's (2004) LSQ approach and an MEM approach to analyzing the data. To measure mean grain size accurately, it was found that many images (10–15) of a sample/location are needed to produce a single stable and dependable mean grain size estimate. The need for large numbers of images comes from both natural variability of sand on a beach as well as the need for high quality images. In particular, image focus needs to be excellent to produce accurate estimates of grain size and when surveying in the surf zone, the motion and battering of the surveyor by the waves can produce many unusable images. Thus, a careful quality control step is necessary for accurate data.

The DIS is capable of producing unprecedented maps of surface grain size in the nearshore. Mean surface grain size has been shown to vary with the morphology, with coarser sediments observed in the deeper rip channels and finer sediments observed on the shoals between the rip channels. The surface sediments high on the beach are even finer, likely owing to sorting through aeolian transport. In addition, where megaripples were actively migrating in a dynamic rip channel, grain size was observed to vary from quite coarse (~0.6 mm) to quite fine (~0.3 mm) over very short distances (~5 m). The patterns were also observed to change with the dynamic, changing bathymetry over the course of the experiment. These temporal changes were observed both with the less frequent large-scale surface grain size surveys and at a single fixed location that was measured on a daily basis. Thus, the DIS has facilitated the observation that sand grain size varies in both space and time on a natural beach.

Acknowledgements

This work was funded by Deltares Coastal Care (Kustlijn zorg), the Office of Naval Research Coastal Geosciences grant N000140510153 and the National Science Foundation grant numbers OCE0340758 and EAR0952164. Funding for AR was provided by National Science

Foundation EAR0952225 and OCE0754426. JM was funded by Office of Naval Research Coastal Geosciences and the National Science Foundation. The video images were made possible by NIWA (New Zealand) and SHOM-DGA (France) with the data processing having been done by Rafael Almar and Vincent Marieu. Early parts of the DIS development were supported (including travel funds and logistics) by Paul Russell and Gerd Masselink (University of Plymouth). Friends and colleagues who also helped enormously include Jeff Brown, Clement Gandon, Martijn Henriquez, Matthieu de Schipper, Marije Smit, Nadia Senechal, Ian Smithgall, Jurre de Vries and Sierd de Vries.

Appendix A. Maximum Entropy Method to estimate grain size distribution

The calibration curves, C_j , have been calculated for discreet grain sizes, D_j (see Section 2.1), according to Eq. (1). Next we use these calibration curves to reconstruct a continuous grain size distribution with the Maximum Entropy Method (MEM) as outlined by Lygre and Krogstad (1986). The reconstruction is restricted to two harmonics, which allows for bi-modal grain size distributions. The continuous grain size distribution is given by:

$$P_{MEM} = A_{MEM} \exp\left(-\sum_{m=1,5} c_m q_m\right)$$

Where:

$$q_1 = 1.0$$

$$q_2 = \sin\left(\frac{2\pi}{D_{max}}D\right)$$

$$q_3 = \cos\left(\frac{2\pi}{D_{max}}D\right)$$

$$q_4 = \sin\left(\frac{4\pi}{D_{max}}D\right)$$

$$q_5 = \cos\left(\frac{4\pi}{D_{max}}D\right)$$

Where D is a grain size array ranging from 0 to D_{max} , with $D_{max} = 2.0$ mm and intervals of 0.05 mm, and c_m represent Lagrangian multipliers. A_{MEM} represents the normalization coefficient such that the area under the P_{MEM} curve equals one.

The grain size fraction, P_j , at the measured grain sizes, D_j , is obtained by interpolation in the normalized grain size distribution P_{MEM} . Next, the mismatch, q , is calculated between the sum of the calibration curves, weighted with their estimated fractions, and the observed auto correlation of the digital image, C_{image} :

$$q = \left(\sum_{j=1,N} P_j C_j - C_{image}\right)^2$$

The estimated distribution (e.g. Fig. 6c and d) is found by minimizing q as function of the Lagrangian multipliers.

References

- Antia, E.E., 1987. Preliminary field observations on beach cusp formation and characteristics on tidally and morphodynamically distinct beaches on the Nigerian coast. *Marine Geology* 78, 23–33.
- Ardhuin, F., Herbers, T.H.C., O'Reilly, W.C., 2001. A hybrid Eulerian–Lagrangian model for spectral wave evolution with application to bottom friction on the continental shelf. *Journal of Physical Oceanography* 31, 1498–1516.
- Ardhuin, F., Drake, T.G., Herbers, T.H.C., 2002. Observations of wave-generated vortex ripples on the North Carolina continental shelf. *Journal of Geophysical Research* 107 (C10), 3143. doi:10.1029/2001JC000986.
- Bagnold, R.A., 1941. *The physics of Blown sand and Desert Dunes*. Methuen and Co. Ltd., London.
- Barnard, P.L., Rubin, D.M., Harney, J., Mustain, N., 2007. Field test comparison of an autocorrelation technique for determining grain size using a digital 'beachball' camera versus traditional methods. *Sedimentary Geology* 201, 180–195.
- Buscombe, D., 2008. Estimation of grain-size distributions and associated parameters from digital images of sediment. *Sedimentary Geology* 210, 1–10.
- Buscombe, D., Masselink, G., 2008. Grain-size information from the statistical properties of digital images of sediment. *Sedimentology* 56, 421–438.
- Castelle, B., Bonneton, P., Dupuis, H., Senechal, N., 2007. Double bar beach dynamics on the high-energy meso-macrotidal French Auitanian Coast: a review. *Marine Geology* 245, 141–159.
- Gallagher, E.L., Elgar, S., Guza, R.T., 1998. Observations of sand bar evolution on a natural beach. *Journal of Geophysical Research* 103, 3203–3215.
- Komar, P.D., 1973. Observations of beach cusps at Mono Lake, California. *Geological Society of America Bulletin* 84, 3593–3600.
- Lippmann, T.C., Homan, R.A., 1989. Quantification of sand bar morphology: a video technique based on wave dissipation. *Journal of Geophysical Research* 94 (C1), 995–1011.
- List, J.H., Farris, A.S., Sullivan, C., 2006. Reversing storm hotspots on sandy beaches: spatial and temporal characteristics. *Marine Geology* 226, 261–279.
- Lygre, A., Krogstad, H.E., 1986. Maximum entropy estimation of the directional distribution in ocean wave spectra. *Journal of Physical Oceanography* 16, 2052–2060.
- MacMahan, J., 2001. Hydrographic surveying from a personal watercraft. *Journal of Surveying Engineering* 127 (1), 12–24.
- MacMahan, J., Reniers, A.J.H.M., Thornton, E.B., Stanton, T.P., 2005. RIPEX: observations of a rip current system. *Marine Geology* 218, 113–134.
- MacMahan, J., Brown, J., Thornton, E.B., 2009. Low-cost handheld Global Positioning Systems for measuring surf-zone currents. *Journal of Coastal Research* 744–754.
- McNinch, J., 2004. Geologic control in the nearshore: shore-oblique sandbars and shoreline erosional hotspots, Mid-Atlantic Bight, USA. *Marine Geology* 211, 121–141.
- Murray, A.B., Thielert, E.R., 2004. A new hypothesis and exploratory model for the formation of large-scale inner-shelf sediment sorting and "rippled scour depressions". *Continental Shelf Research* 24, 295–315.
- Rubin, D.M., 2004. A simple autocorrelation algorithm for determining grain size from digital images of sediment. *Journal of Sedimentary Research* 74, 160–165.
- Rubin, D.M., Topping, D.J., 2001. Quantifying the relative importance of flow regulation and grain-size regulation of suspended-sediment transport (α) and tracking changes in grain size on the bed (β). *Water Resources Research* 37, 133–146.
- Rubin, D.M., Chezar, H., Harney, J.N., Topping, D.J., Melis, T.S., Sherwood, C.R., 2007. Underwater microscope for measuring spatial and temporal changes in bed-sediment grain size. *Sedimentary Geology* 202, 402–408.
- Senechal, N., Gouriou, T., Castelle, B., Parisot, J.-P., Capo, S., Bujan, S., Howa, H., 2009. Morphodynamic response of a meso- to macro-tidal intermediate beach based on a long-term data set. *Geomorphology* 107, 263–274.
- Tolman, H.L., 1994. Wind waves and moveable-bed bottom friction. *Journal of Physical Oceanography* 24, 994–1009.
- Trembanis, A.C., Wright, L.D., Friedrichs, C.T.M.O., Green, M.O., Hume, T., 2004. The effects of spatially complex inner shelf roughness on boundary layer turbulence and current and wave friction: Tairua embayment, New Zealand. *Continental Shelf Research* 24, 1549–1571.